Ripples in a wetting film formed by a moving meniscus

Vladimir S. Ajaev
Department of Mathematics, Southern Methodist University, Dallas, Texas 75275, USA

Roumen Tsekov
DWI, RWTH Aachen, Pauwelsstrasse 8, 52056 Aachen, Germany

Olga I. Vinogradova
A.N. Frumkin Institute of Physical Chemistry and Electrochemistry, Russian Academy of Sciences, 31 Leninsky Prospect, 119991 Moscow, Russia

(Received 5 June 2008; published 12 September 2008)

We carry out a theoretical investigation of the evolution of a wetting film formed by pressing a bubble against a solid substrate. Our model incorporates the effects of capillarity and Derjaguin-Landau-Verwey-Overbeek (DLVO) (van der Waals and electrostatic) components of the disjoining pressure. Rapid changes in the relative position of the bubble and the substrate are shown to result in surprisingly rich dynamics of wetting film deformations. Even for stable films, we find transient rippled deformations with several points of local maximum of wetting film thickness and discuss how their evolution depends on changes in the meniscus position relative to the substrate and the disjoining pressure parameters. A connection is made to the recently reported experimental observations of one such rippled deformation, the so-called wimple, characterized by a local minimum of the thickness in the center, surrounded by a ring of greater film thickness and bounded at the outer edge by the barrier rim. Guidelines are provided for experimental detection of more complex rippled deformations in stable wetting films. Development of instability is studied in a situation when the electrostatic component of disjoining pressure is destabilizing, with particular emphasis on the nonlinear evolution and rupture of the film. Potential applications of our findings to small-scale mixing and deposition of nanoparticles are discussed.

DOI: 10.1103/PhysRevE.78.031602 PACS number(s): 68.15.+e, 47.61.−k

I. INTRODUCTION

Studies of thin liquid films are important for understanding the flotation process, behavior of emulsions, and dynamics of confined drops and bubbles in microfluidic devices. A well-studied experimental configuration involves a draining film formed when a bubble or a liquid drop surrounded by another viscous liquid is pressed against a solid wall. It has been known for decades that the hydrodynamic pressure in the film can be large enough to invert the curvature of a fluid drop or a bubble by forming the so-called dimple [1–3]. The dimple is bounded by a barrier rim, which is the circle of minimum separation between the two surfaces. Mathematical models have been developed to describe dimple formation and estimate the rate of liquid drainage in this configuration on the macroscopic scale [4–7]. When the draining film thickness is sufficiently small (on the order of 100 nm or less), the effect of disjoining pressure becomes important [8,9]. Yiantsios and Davis [10] developed a theoretical model of the drainage of a film between two fluid interfaces that included the effect of the van der Waals component of disjoining pressure. Hewitt *et al.* [11] studied the effect of the electrostatic component of disjoining pressure on aqueous film drainage between an air bubble and quartz substrate using scanning optical interferometry. Connor and Horn [12] conducted careful experimental studies of aqueous film draining between a mercury droplet and a substrate, also in a situation when electrical double layer forces are significant. Inclusion of disjoining pressure changes the quantitative details and improves the comparison between theory and experiment, but the main qualitative features of the dimple formation turn out to be similar to the macroscopic case. A more detailed review of literature on dimples in draining films can be found, e.g., in Slattery *et al.* [13].

While dimples have been studied extensively, they are not the only shapes that can be observed in draining stable films, as was first shown experimentally by Clasohm *et al.* [14]. In their experimental setup an air bubble or mercury drop in aqueous solution is pressed against a wall as sketched in Fig. 1, and the wetting film profile is measured using multiple beam interferometry in the reflection mode. Clasohm *et al.* [14] found that if the substrate starts to move towards a drop or bubble from an equilibrium configuration, a complex rippled shape, referred to as a wimple, can be observed at the initial stage of approach. In a wimple, the drop or bubble surface buckles into a depressed ring with the central peak,

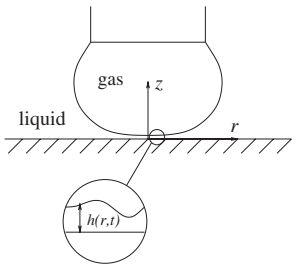

FIG. 1. Sketch of a bubble attached to a capillary and pressed against a solid surface. The enlarged portion of the film illustrates wimple, which is one of several possible shapes of draining film.

as seen in the enlarged view of the draining film in Fig. 1. This shape later evolves to a conventional dimple, which then drains in the usual way. These experiments clearly showed that the commonly accepted notions about the shape evolution of a draining film are incomplete and that more theoretical studies are needed to interpret the new experiments. The first such study was conducted by Tsekov and Vinogradova [15], based on the analysis of interfacial stress conditions under the assumption that the draining film is nearly flat, i.e., the amplitude of deformations is small compared to the average film thickness. It was shown that complex rippled deformations of thin films can arise due to an interplay between surface tension and disjoining pressure. The focus of the present study is on numerical simulations of nonlinear evolution of complex rippled deformations whose amplitude is comparable to the average wetting film thickness, so that linearized theories are not sufficient to describe film evolution.

It is important to note that rippled dissipative structures in thin films have been observed by a number of researchers, but they were attributed to various types of instabilities [16–19]. The striking aspect of the experimental results of Clasohm *et al.* [14] is that such structures are seen in stable nanofilms, where surface tension and positive disjoining pressure corresponding to repulsive interaction between the fluid interface and the solid, are expected to suppress any wavelike deformations. The physical mechanism of this phenomenon was explained by Ajaev *et al.* [20] using a simple model that involves only capillarity and van der Waals–type disjoining pressure. When the distance between the bubble and the substrate is changed, the thin-film region is expanded due to formation of a trailing film behind shifted meniscus. The pressure in the trailing film is lower than the pressure in the meniscus region and in the static wetting film; the flow of liquid from this region of relatively high pressure causes the interface deformation. In the present work, the effect of the electrostatic component of disjoining pressure on wimple formation is investigated and extensive parametric studies are conducted to obtain the conditions of wimple formation. Furthermore, new types of interface shapes in draining films are found from numerical simulations. Simple physical explanations and analytical formulas for conditions of formation of these shapes are provided. The rate of viscous flow in the film is studied as a function of bubble motion relative to the substrate.

Significance of the experimental discovery made in Ref. [14] goes beyond the particular experimental setup discussed there. Any kind of situation where a macroscopic meniscus is initially in contact with an equilibrium wetting film and then starts moving is expected to result in the same dynamics. Such situations are often encountered in studies of moving contact lines [21]. Thus, the work of Clasohm *et al.* [14] can have important implications for theoretical prediction of values of apparent contact angles.

In the classical studies of drainage based on the setup of Fig. 1 the deformations of bubbles happen on a relatively slow time scale compared to those observed in microfluidic devices, in which drops and bubbles are often going though constrictions and bouncing against the confining walls [22]. The present work is an important step towards understanding interactions of drops and bubbles with solid boundaries in such dynamic situations.

The paper is organized as follows. Formulation is presented in Sec. II. Numerical studies of wimples and criteria for their formation are described in Sec. III. More complicated rippled interface shapes and film instability induced by the disjoining pressure are discussed in Sec. IV. Finally, the key findings are summarized in Sec. V.

II. FORMULATION

Consider an axisymmetric bubble pressed against a horizontal rigid surface, which is a typical experimental configuration [11,14,23], illustrated in Fig. 1. Liquid has viscosity μ and surface tension at the liquid-gas interface is σ. The bubble is held at the end of a fixed vertical capillary, while the solid substrate can be moved in the vertical direction at a controlled velocity $V(t)$. When the bubble is far from the solid wall, its radius of curvature is constant and equal to R_0, assuming that gravity can be neglected, i.e., the Bond number is small. When the bubble is close to the wall its shape is distorted locally by surface and hydrodynamic forces, resulting in the formation of a liquid film between the gas and the solid. When the substrate moves toward the capillary, the film region expands at a rate characterized by the velocity of its outer edge U used as the horizontal velocity scale in our model. The corresponding capillary number $C=\mu U/\sigma$, is assumed to be a small parameter here since its values in typical experiments are $\sim 10^{-6}$ or even smaller. The interplay between viscous flow and surface tension in the thin liquid film for small C is described by the so-called Landau-Levich-Bretherton scaling [21,24], which in the present context implies using $C^{1/3}R_0$ and $C^{2/3}R_0$ as the length scales in the radial and vertical directions, respectively. The scaled cylindrical coordinates r and z are shown in Fig. 1. The position of the liquid-gas interface is characterized by the scaled film thickness $h(r,t)$, where t is the time variable scaled by $C^{1/3}R_0/U$.

To develop an asymptotic theory we expand the governing equations and boundary conditions in the powers of the small parameter $C^{1/3}$. At the leading order, the governing equations take the usual lubrication-type form [25] while the boundary conditions of normal and shear stress balances at the gas-liquid interface are written as

$$p_g - p = h_{rr} + r^{-1}h_r + \Pi(h), \tag{1}$$

$$u_z = 0, \tag{2}$$

where p_g and p are the scaled pressures inside the bubble and in the liquid film, respectively, $\Pi(h)$ is the disjoining pressure; all three are scaled by σ/R_0 and u is the horizontal velocity scaled by U. Here and below we use the expression for disjoining pressure in the DLVO form [8,9]

$$\Pi = \alpha h^{-3} + \beta e^{-\chi h}, \tag{3}$$

where $\alpha=-A/\sigma C^2 R_0^2$ and A is the Hamaker constant. The first term is the London–van der Waals component of disjoining pressure, the second is the electrostatic component char-

acterized by two nondimensional parameters β and χ. The latter is inversely proportional to the Debye length. This model is adequate for describing the situation relevant for many experiments [23,26] and was used for theoretical studies [27,28], although other disjoining pressure models are also used in the literature, e.g., a combination of two terms which are different inverse powers of h [29,30].

The standard lubrication-type velocity profile [25] is substituted into the integral form of the mass conservation condition resulting in the following equation for the scaled liquid film thickness $h=h(r,t)$

$$h_t + (3r)^{-1}[rh^3(h_{rr} + r^{-1}h_r + \alpha h^{-3} + \beta e^{-\chi h})_r]_r = 0. \quad (4)$$

The boundary conditions for this equation at $r=0$ are the conditions of axial symmetry expressed by

$$h_r(0,t) = 0, \quad h_{rrr}(0,t) = 0. \quad (5)$$

The size of the computational domain, L, is chosen sufficiently large so that the effect of disjoining pressure on the interface shape near $r=L$ is negligible, i.e., the value $\Pi[h(L,t)]$ is small for all t. At $r=L$ we specify the vertical velocity of the interface (as, e.g., in Ref. [31]) and the value of curvature corresponding to the meniscus away from the draining film region. The general form of these two conditions is

$$h_t(L,t) = -V(t), \quad h_{rr}(L,t) + L^{-1}h_r(L,t) = \kappa(t). \quad (6)$$

The value of the curvature away from the film $\kappa(t)$ is taken to be 1 in most of our simulations below. This is justified by the fact that away from the film the interface shape is dominated by the capillary forces and therefore its curvature does not change significantly as the bubble is shifted, generating flow in the liquid. This assumption is supported further by the experimental recordings of interface shapes and by the fact that pressure gradient in draining flows is known to decay as r^{-5} for large r [32].

Equation (4) with the specified boundary conditions was solved numerically using a finite difference approach with time stepping based on Gear's backward differentiation formulas [33]. Analytical formulas are incorporated into the code for evaluating the curvature and its derivatives at $r=0$.

III. WIMPLES IN DRAINING FILMS

A. Mechanism of interface deformation

When a bubble is pressed against the wall, as seen in Fig. 1, the disjoining pressure in the wetting film balances the capillary pressure jump across the meniscus surface, so that the overall configuration is steady. This configuration is taken as the initial condition in our numerical simulation. To simulate the steplike substrate motion toward the bubble, the height on the right end of the computational domain decreases at a constant rate $V(t)=1$ from the initial value of $h(L,0)=8$ over the time period of $\Delta t=5$. We note that in experiments of Clasohm *et al.* [14] the bubble is attached to the capillary and the relative velocity of the capillary and the substrate is held constant during the steplike approach, which is in contrast to drainage under the conditions of constant

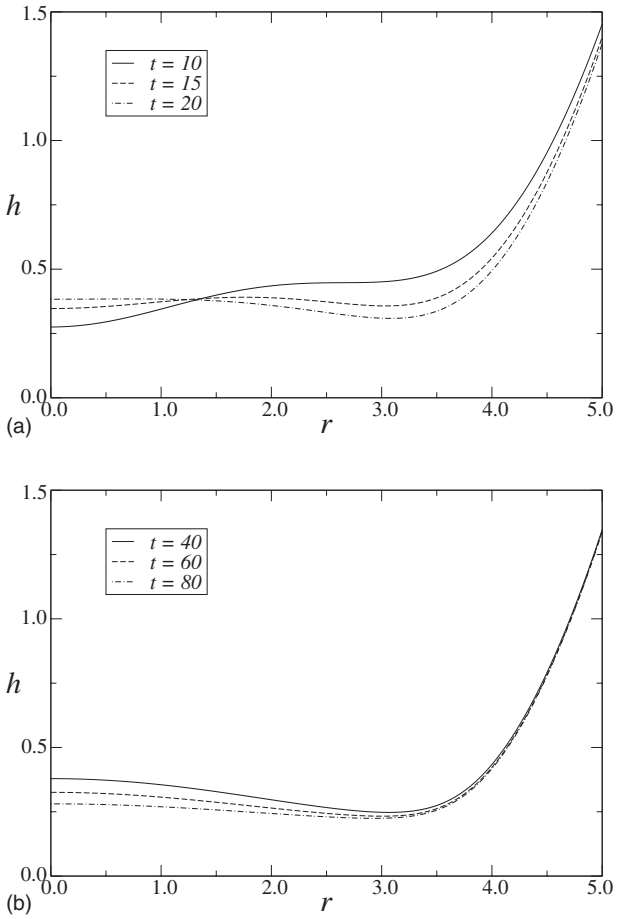

FIG. 2. Numerical results for $\alpha=10^{-3}$, $\beta=50$, $\chi=20$ illustrating liquid-gas interface evolution: (a) formation of the wimple; (b) drainage of the dimple at the later stages of evolution.

interaction force, i.e., due to buoyancy. Figure 2(a) shows typical simulation results [for $\alpha=0.001$, $\beta=50$, $\chi=20$, $\kappa(t)=1$, $L=6$] at the initial stages of the process. Snapshots of the interface are recorded at three different values of scaled time t specified in the legend. As the outer edge of the thin-film region shifts to the right, a local depression away from the central axis develops in the newly formed liquid film, resulting in a shape with a minimum at the axis of symmetry and the second minimum at a finite r. This shape is referred to as the wimple.

At later stages of evolution the wimple transforms into the standard dimple shape [32,34,35] and the latter slowly relaxes to the flat film, as illustrated in Fig. 2(b). This turns out to be a much slower process than the initial evolution. The minimum value of the film thickness decreases initially and then does not change significantly at later stages of drainage. The film becomes nearly flat at $t \sim 10^2$.

A simple explanation of wimple formation was proposed in our earlier study [20]. Even though the model of disjoining pressure in the present study is different from Ref. [20], the mechanism of the interface deformation is essentially the same. In equilibrium, the disjoining pressure in the wetting film balances the capillary pressure jump across the meniscus surface. When the meniscus starts moving, the trailing film is formed by the Landau-Levich-type mechanism; the

typical thickness of this film scales as $C^{2/3}$ and is usually larger than the wetting film thickness [as seen in the flattened portion of the solid curve in Fig. 2(a)]. Thus the disjoining pressure in this region is relatively weak. However, so is the capillary pressure jump, since the trailing film is almost flat when it is just formed. As a result liquid is pushed out of this region in both directions, i.e., toward the capillary meniscus region and toward the wetting film, resulting in formation of the wimple. Note that the liquid flow during wimple formation is directed towards the central axis in parts of the film before draining in the opposite direction later [14]. This is in contrast to the many numerical simulations of dimple formation that do not show flow reversal.

We note that the steplike changes in the velocity $V(t)$ used in our simulations imply infinitely large acceleration of the interface and therefore raise the issue of validity of our model. To address this issue, we carried out several simulations for large but finite rate of change of velocity and found that the behavior of the draining film over the time scales of interest does not change significantly. This can be explained by the fact that the evolution of the film discussed in the present study takes place after the substrate stopped moving, so it is not particularly sensitive to the details of how the substrate was accelerated or stopped as long as the amount of shift is the same. We also ran several simulations with various nonconstant $\kappa(t)$ that simulate slight flow-induced changes of curvature of moving bubble and found that the dynamics of wetting film is not very sensitive to small variations of $\kappa(t)$.

B. Wimple versus dimple

Numerical simulations of the interface evolution, such as the one illustrated in Fig. 2, show that wimple is formed at a certain time $t_w > 0$ following the change in the distance between the bubble and the substrate initiated at $t=0$. Let us investigate how t_w depends on disjoining pressure. In many experiments the disjoining pressure is dominated by its electrostatic component, which is defined by two parameters β and χ in our model. Let us first vary the constant β, which measures the significance of this component and depends on the electrostatic potentials of the solid-liquid and liquid-gas interfaces. A typical result (for fixed van der Waals component of disjoining pressure, defined by $\alpha=0.001$, and for fixed $\chi=20$) is shown in Fig. 3(a). Clearly, the decrease in the disjoining pressure parameter results in delayed wimple formation. This can be explained by the fact that for smaller β the equilibrium film thickness is smaller and therefore the viscous resistance is more significant compared to the effect of pressure jump at the interface. The latter is the driving force for the flow and depends on both surface tension and disjoining pressure. The slowdown of the film evolution due to increased role of viscous friction at smaller β is not a dramatic effect: t_w changes by less than 10% over a wide range of β shown in Fig. 3(a).

In experiments, the electrostatic component of disjoining pressure can be controlled by changing the concentration of ions in the liquid so that the Debye length changes. In our model, the parameter χ^{-1} is proportional to the Debye length,

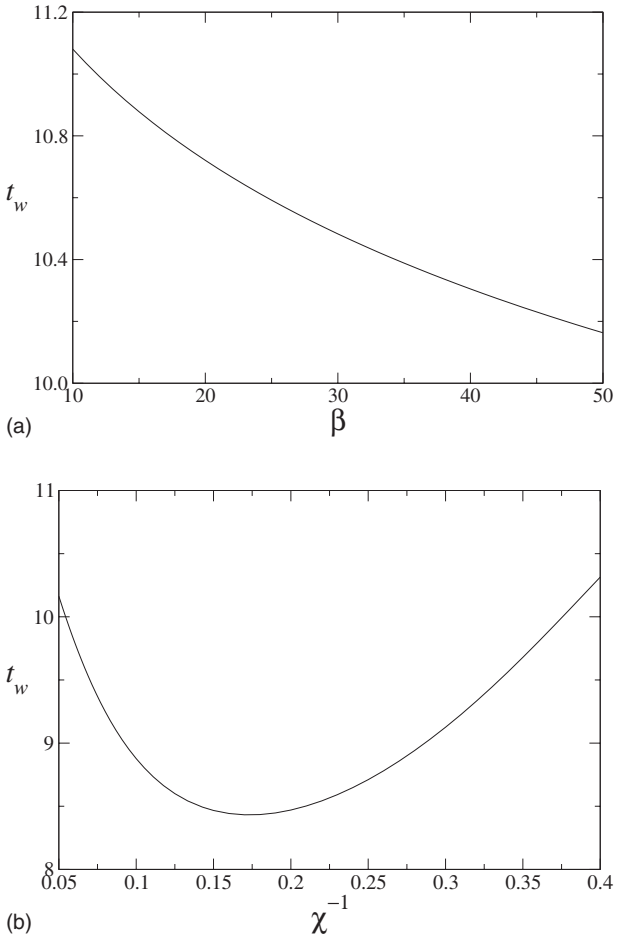

FIG. 3. The effect of disjoining pressure variations on film evolution. The nondimensional time of wimple formation for $\Delta t=5.0$ is shown as a function of β (a) and as a function of χ^{-1} with fixed $\beta\chi^{-2}=0.125$ (b).

but β also depends on it. In fact, variation of the ion concentration implies changing both χ and β but in such a way that $\beta\chi^{-2}=$const [9]. The result for $\alpha=10^{-3}$ is shown in Fig. 3(b). Comparison between the two parts of Fig. 3 shows that t_w is more sensitive to variations in χ than variations in β, which can be explained by the strong (exponential) dependence of disjoining pressure at a given thickness on χ. The time of wimple formation is minimized at the maximum value of the equilibrium wetting film thickness, corresponding to $\chi^{-1} \approx 0.17$.

Let us investigate how the dynamics of wimple formation depends on the amount of shift in the distance between the bubble and the substrate, which is a natural control parameter in experiments. In our model the amount of shift is measured by the nondimensional parameter Δt. The result for the nondimensional time of wimple formation t_w versus Δt is shown in Fig. 4 for typical disjoining pressure parameters $\alpha=0.001$, $\beta=50$, $\chi=20$. Somewhat unexpectedly, the plot of t_w has a maximum at a certain value of Δt. This may seem counterintuitive since according to the mechanism of wimple formation discussed in the previous subsection, larger Δt implies larger extent of the trailing film and therefore should promote faster wimple formation. However, this reasoning

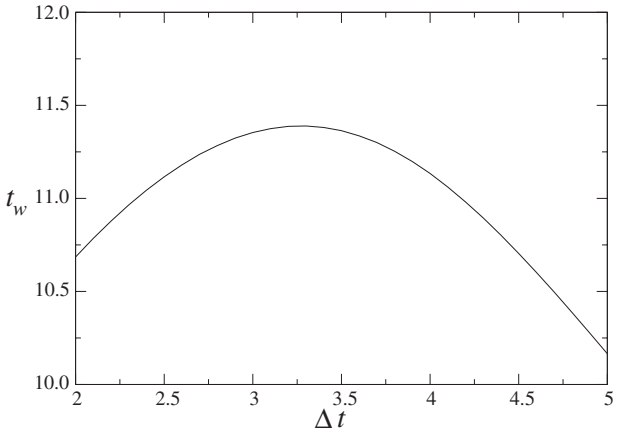

FIG. 4. Nondimensional time of wimple formation as a function of Δt for $\alpha=0.001$, $\beta=50$.

does not take into account the fact that wimples seen at larger Δt have larger amplitude (the difference between the maximum and minimum values) and width than the ones formed at smaller Δt. The latter ones appear and then turn to dimples very quickly, which is also an indication that they may be difficult to detect experimentally.

It is important to note that for sufficiently small Δt the wimple, which is always a transient shape, is not formed at all. In order to be able to detect wimples in experiments, it is important to specify criteria for their formation. In the framework of our model such criteria can be easily formulated in terms of the nondimensional parameters Δt and β. The diagram in Fig. 5, found from extensive numerical studies, gives the conditions for wimple formation. A dimple and/or a flattening of the film represents the only type of evolution for parameter values corresponding to Δt and β below the solid curve in Fig. 5 while wimple can be observed above the curve. To generate the plot in Fig. 5, our numerical algorithm monitored interface shape up to a point t_m when a local minimum of the draining film thickness first appeared at an off-center location $r_1>0$ and evaluated the difference $h(r_1,t_m)-h(0,t_m)$. Wimple was detected when this value was above 10^{-4}.

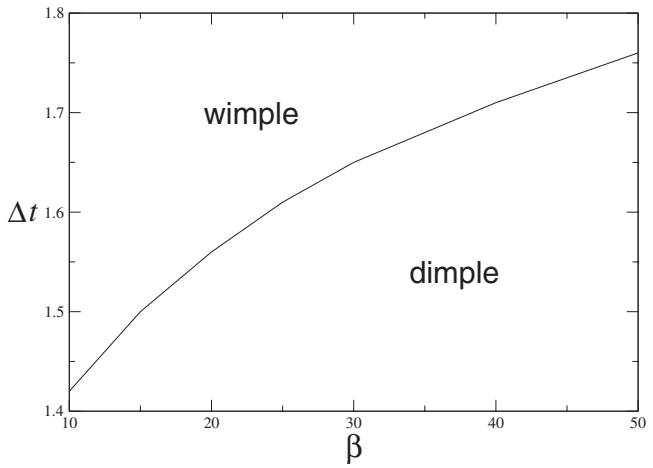

FIG. 5. Minimum Δt for wimple formation versus the disjoining pressure parameter. Wimple is not formed for small Δt.

Let us now discuss the connection of the present model to experiments. In typical experiments with bubbles or drops pressed against solid substrates the size R_0 is of the order of 1 mm and the values of $C^{1/3}$ at realistic speeds are $10^{-3}-10^{-2}$, which is of the same order as typical inverse aspect ratios of the draining films, thus justifying our lubrication-type approach. In the experiments of Clasohm *et al.* [14] wimple shapes were detected using the setup of Fig. 1 and a similar setup with a droplet of mercury instead of air bubble. Detailed measurements of interface evolution were shown only for the latter case, which makes it difficult to make direct quantitative comparisons with our model. However, the mechanism discussed in the previous section suggests that qualitative comparison can still be made since the limiting mechanism of interface evolution is expected to be due to viscous flow in the thin-film region, with flow inside the droplet playing a secondary role. Thus, the experimentally observed trends should be consistent with the predictions of our model. Let us show that this is indeed the case.

Clasohm *et al.* [14] investigated evolution of draining film for four different values of the shift ΔL^* in the relative position of the substrate and the capillary tube to which the drop/bubble is attached. Based on their data, the time of wimple formation is estimated to be near 0.3 s for $\Delta L^*=20$ μm and near 0.4 s for $\Delta L^*=10$ μm, which is clearly consistent with the decaying part of the curve in Fig. 4 (note that in our model the shift in position is measured by Δt). As we discussed above, the growing part of the plot in Fig. 4 corresponds to short-lived wimples of very small amplitude, likely to be difficult to detect. Clasohm *et al.* [14] also discovered that the wimple is formed for ΔL^* above a critical value, which they estimated to be between 5 and 10 μm. Our condition of wimple formation, illustrated in Fig. 5, estimates the critical value to be on the order of several microns (when the capillary number is evaluated based on the surface tension of water-mercury interface used in Ref. [14]). When making the comparison, it is important to account for the difference between the experimentally controlled ΔL^* and the dimensional change in the interface height $C^{2/3}R_0\Delta t$. The latter can be estimated for a given ΔL^* by analyzing the capillary statics shapes of the bubble/drop before and after the shift or can be extracted from the experimental recordings of the film surface shapes. Both approaches indicate that ΔL^* is typically an order of magnitude larger than $C^{2/3}R_0\Delta t$. To complete the comparison with experiments, we note that our numerical results, such as the one seen in Fig. 3(a), predict slower evolution of the draining film for smaller β. This is indeed observed in experiments [14]: weaker repulsion case (corresponding to smaller β in our model) corresponds to slower film evolution than the strong repulsion case.

Manica *et al.* [36] recently used an approach to modeling of draining films similar to Ajaev *et al.* [20] and the present work, except that instead of the zero shear-stress condition they postulated no slip at the fluid interface. (Note that although the treatment of the far-field boundary conditions in Ref. [36] is slightly different from the one we use here, both are adequate for correctly capturing the evolution of the wetting film.) It is interesting that despite the modification of interfacial boundary condition, the results of Manica *et al.* are also consistent with the experimental data of Clasohm *et*

al. [14] obtained with the mercury drop, as well as with our early theoretical conclusions [15,20] made for a bubble. This confirms the universality of the physical mechanism of a wimple formation proposed in Ref. [20].

While the experimental results of Clasohm *et al.* [14] provide important verification of the key aspects of our model, more experimental work is needed to test our predictions. The present theoretical work provides a number of useful guidelines for future experimental studies, most notably the conditions for wimple formation when a gas bubble is pushed against a solid substrate.

IV. MULTIPLE DIMPLES

A. Two-step forcing

Simulations in the previous section are conducted for situations when the initial condition ($t=0$) is an equilibrium configuration (which in practice takes a long time to achieve). Let us investigate what will happen when the change in the velocity is made as the draining film approaches the equilibrium state. To simulate this situation we use the two-step velocity profile defined by

$$V(t) = \begin{cases} 1, & 0 < t < \Delta t, \quad t_1 < t < t_1 + \Delta t, \\ 0, & \text{otherwise}. \end{cases}$$

Snapshots of interface shapes for this profile with $\alpha=0.001$, $\beta=50$, $\chi=20$, $\Delta t=3.5$, $t_1=6\Delta t$ are shown in Fig. 6(a). A new transient shape with two off-center points of minimum is seen in this simulation: we refer to such shapes as multiple dimples. Although the linear analysis of small transient deformations of a draining film conducted by Tsekov and Vinogradova [15] suggested that shapes with several minima can appear, no previous observations of such shapes in numerical simulations of the full nonlinear evolution equation were reported in the literature. The multiple dimples we observe are short-lived, turning to wimples and then to dimples. Thus, there is a sequence of transient shapes in the nonlinear evolution of the liquid-gas interface.

While multiple dimples are typically short-lived structures, increasing the value of Δt can help to bring the systems into a regime when they persist for longer time. This is seen in the plot of time t_{MD} of the evolution of multiple dimples versus Δt in Fig. 6(b). For values of Δt below ~ 3.3 in the plot multiple dimples are not formed.

The mechanism of multiple dimple formation is illustrated in Fig. 7. At time near $t=t_1$, the shape of the interface can be described as a slowly draining dimple, shown in the top part of Fig. 7, with the pressure near the point A slightly above the pressure at the point B. As the meniscus is shifted, the trailing-film region is formed near B. Since the trailing film is nearly flat and thicker than the minimum thickness of the wetting film, both capillary pressure jump and disjoining pressure are relatively weak in the trailing film. Thus, the pressure in the region B is higher than the pressures in regions A and C shown in the sketch and liquid flows away from B, resulting in formation of a local minimum of the draining film thickness near B. The overall shape of the interface at this stage is what we refer to as multiple dimple.

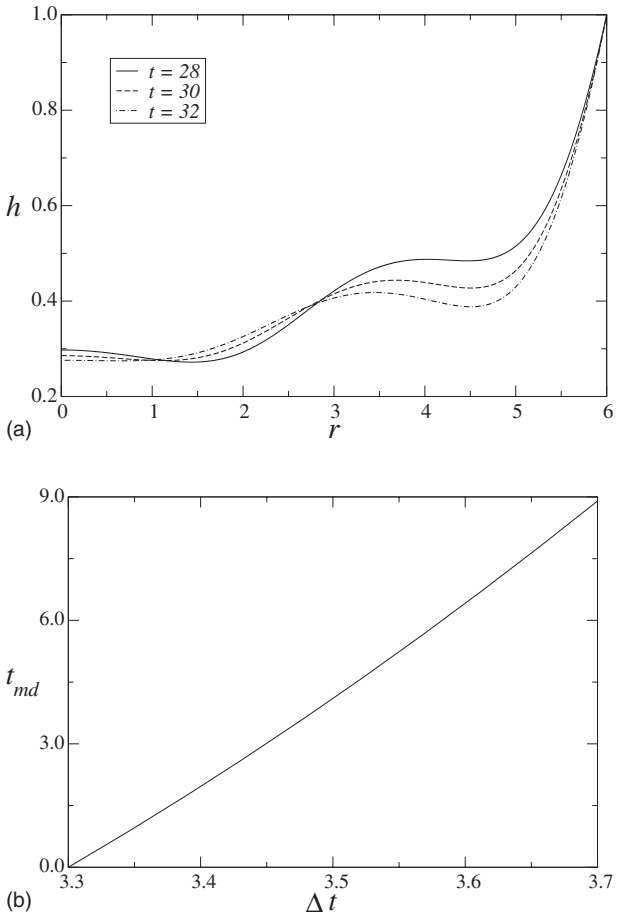

FIG. 6. (a) A sketch of a multiple dimple seen in numerical simulations. (b) Nondimensional time of multiple dimple evolution.

Approximate analytical solutions describing the formation of these rippled structures are given in the Appendix.

Experimental studies [23] indicate that disjoining pressure can change from repulsive to attractive at small separations, due to rearrangement of electrical charges. Such situation may result in film rupture. In order to model film evolution for attractive electrostatic component of disjoining pressure without dealing with the difficulties associated with description of newly formed contact line, we consider the case when the film gets stabilized by van der Waals forces at very small

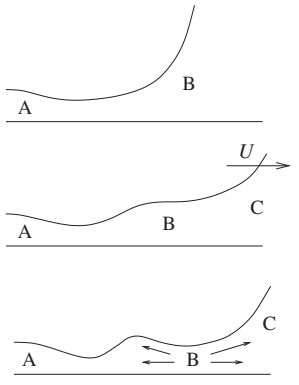

FIG. 7. Illustration of the mechanism of formation of multiple dimples in wetting films.

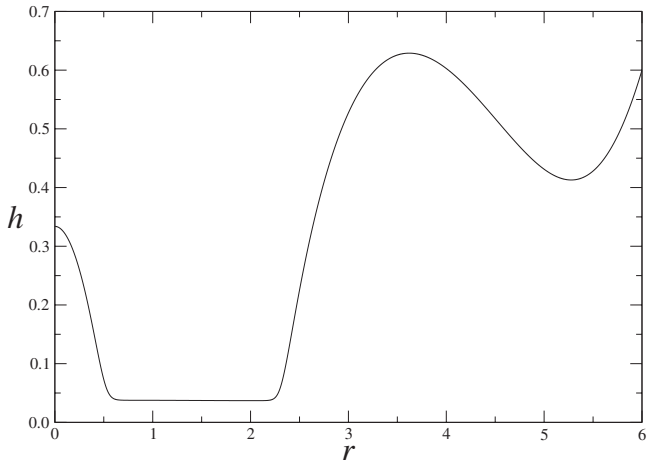

FIG. 8. Interface shape at $t=28$ found from the simulation with $\alpha=0.001$, $\beta=-50$.

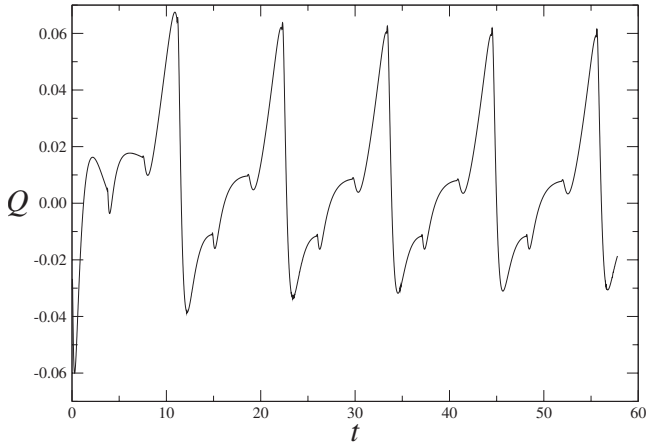

FIG. 9. Dynamic response of the periodic flow in the film to periodic variations in the distance between the bubble and the substrate.

thickness. The result in Fig. 8 (for $\alpha=10^{-3}$, $\beta=-50$, $\chi=20$) shows a structure that can be described as in isolated droplet in the middle, with a ring of liquid forming at an off-center location (the same two-step velocity profile as above was used in this simulation). This result indicates that by repeating the process several times one can make a pattern of circles on a substrate, which is significant for many applications. The liquid can be solidified afterward, resulting in a highly ordered nanostructured surface. Furthermore, if the liquid is a suspension of nanoparticles, the effect can potentially be used for deposition of highly ordered rings of nanoparticles or self-assembly from DNA solutions. These have important potential applications in optics and biology [37,38].

B. Dynamic response

Controlling the flow in the film of typical thickness of tens of nanometers is a difficult task, but it is important for many applications in microfluidics and nanofluidics. The setup of Fig. 1 offers remarkable opportunities for controlling the flow in ultrathin films. However, in order to use it for practical applications it is important to establish the relation between the shift in the relative position of the bubble and the substrate on one hand and the flow in the film on the other, i.e., study the response of the film to external forcing though the meniscus. A typical result of such study is illustrated in Fig. 9, where we plot the liquid flow rate at $r=2$ as a function of time for periodically changing distance between the bubble and the substrate. It is clear that both the magnitude and the sign of the flow rate in the film change at each step. After a very short transient period, a periodic solution is established. The rapid decay of transients can be explained by the significance of viscous forces in films of such small thickness. We note that the periodic nature of the solution seen here is due to periodic forcing. More complicated flow can be induced by nonperiodic forcing.

Figure 9 illustrates that by rapidly pushing the bubble toward a solid wall one can quickly induce and then control a flow in the thin film formed between the bubble and the wall. This effect can be used in applications such as mixing in small-scale systems. The actual design of such mixing device is beyond the scope of the present paper and can involve a more complicated geometric configuration than a bubble attached to a tube.

V. CONCLUSIONS

We carried out a theoretical investigation of the effects of capillarity and both van der Waals and electrostatic components of disjoining pressure on evolution of a wetting film formed by pressing a gas bubble against a solid substrate. We first model the situation when deformations and liquid flow in stable wetting films are induced by changing the position of the bubble relative to the substrate, e.g., by pushing the bubble toward the substrate. When the bubble is moved a fixed distance from an equilibrium configuration, a transient shape seen in the simulation has a local minimum of the thickness in the center, surrounded by a ring of greater film thickness and bounded at the outer edge by the barrier rim. This has recently been discovered experimentally and is referred to as the wimple. Our study is the first one to derive the conditions of wimple formation and its evolution time as functions of the amount of shift in the bubble position and the parameters of disjoining pressure. In particular, we find that wimple is formed faster for weaker disjoining pressure. Our results are consistent with experimentally observed trends and provide useful guidelines for future experiments.

Our numerical simulations allowed us not only to reproduce wimples and their evolution to conventional dimples, but also obtain new kinds of transient interface shapes, dubbed "multiple dimples." These emerge when the bubble is pushed toward the substrate more than once. Physics of new transient interface shapes is explained in terms of interplay between capillarity and disjoining pressure. Simple analytical estimates are provided to validate the explanations. Our simulations clearly indicate that the shifts in the position of the macroscopic bubble (relative to the substrate) can be used to control flow and deformations in nanoscale films.

In addition to interface shapes, we have investigated the flow in the ultrathin liquid film. A remarkable finding here is that the flow direction can be effectively controlled by the motion of the bubble. In particular, we showed that rapid periodic reversal of the flow direction can occur as a result of oscillatory motion of the meniscus. The ability to rapidly induce flow in ultrathin films can be useful for mixing in such a small-scale system.

When the electrostatic component of disjoining pressure is destabilizing, the motion of the meniscus has a significant effect on the development of instability. This situation is different from the one corresponding to stable film because the flow is induced not just by motion of the bubble but also by the destabilizing effect of disjoining pressure. In particular, when the growing perturbation is defined by the prescribed motion of the meniscus, the rippled structure can result in an ordered pattern of rings on the surface. This can be used to manufacturing the patterned surface (when the liquid solidifies after the rings are formed) or for deposition of nanoparticles (when the liquid contains nanoparticles and it dries out by evaporation after the rings are formed on the substrate).

ACKNOWLEDGMENTS

This work was partly supported by a DFG priority program "Micro and nanofluidics" (Grant No. Vi 243/1-3) and by a grant from the NSF.

APPENDIX: LINEARIZED THEORY OF RIPPLES IN THE FILM

Approximate analytical formulas can be used to determine the conditions of formation of dimples, wimples, and more complicated multiple dimple structures. Indeed, the linearized analysis of Eq. (4), based on Ref. [15], indicates that the interface deformation can be described by

$$h_t + (3r)^{-1}\bar{h}^3[r(h_{rr} + r^{-1}h_r - 3\alpha\bar{h}^{-4}h - \beta\chi e^{-\chi\bar{h}}h)_r]_r = 0, \tag{A1}$$

where $\bar{h}$ denotes the average film thickness. The solution of Eq. (A1) on $[0,L]$ can be written as a linear superposition in the form

$$h = \bar{h} + \sum_n A_n e^{-\gamma_n t} J_0(q_n r). \tag{A2}$$

Since the average value of the sum over n on the right-hand side has to vanish, the dimensionless wave numbers q_n obey the relationship $J_1(q_n L)=0$, based on the well-known relation between Bessel functions of the zeroth and the first orders. Thus, $q_n=\lambda_n/L$, where λ_n is the nth root of the Bessel function of the first kind J_1. The dimensionless decay rate γ_n satisfies the following dispersion relation:

$$\gamma_n = \frac{\bar{h}^3 q_n^2}{3}(q_n^2 + 3\alpha\bar{h}^{-4} + \beta\chi e^{-\chi\bar{h}}). \tag{A3}$$

In general all the Fourier components are present at a given time t. However, the components with fast decay rate do not contribute substantially to the film profile, since they relax very quickly, i.e., $e^{-\gamma_n t}$ in Eq. (8) is small if $\gamma_n \gg t^{-1}$. At very large times the film reaches flat equilibrium shape, which corresponds to perturbations of all wavelengths decaying to zero. At the late stages of the shape evolution (relatively large t), the film is not yet at equilibrium, but already close to it. Thus, the Fourier components with large γ_n are also decaying, but the film is not flat yet due to the component $n=1$. Then the interface shape is essentially dimpled with a characteristic wave number $q_1=\lambda_1/L$. Since $\lambda_1 \approx 3.83$, the dimple has a maximum in the film center and a minimum at the rim. If we now consider the shape evolution before the dimple formation one could expect that $q_2=\lambda_2/L$ will also play an important role. The value $\lambda_2 \approx 7.02$ corresponds to a wimple with a maximum surrounded by two minima at the center and the rim. Finally, formation of multiple dimples corresponds to $q_3=\lambda_3/L$, where $\lambda_3 \approx 10.17$. We note that the simple analytical estimates based on these values are in good agreement with the results of our numerical simulations.

In Ref. [15] transitions between different interface shapes were discussed based on the assumption that the interface shape is dominated by a single Fourier component of the superposition given by Eq. (A2); the wave number of that component was denoted by $\sqrt{b}$ in Ref. [15]. The multiple dimple and wimple shapes then correspond to larger values of b, while dimple is expected at smaller b, with the transition between the two taking place when b is near the square of the first root of the Bessel function J_1.

[1] B. V. Derjaguin and M. M. Kussakov, Acta Physicochim. URSS **10**, 25 (1939).
[2] D. Platikanov, J. Phys. Chem. **68**, 3619 (1964).
[3] S. Hartland, Chem. Eng. Sci. **65**, 82 (1969).
[4] S. P. Frankel and K. J. Mysels, J. Phys. Chem. **66**, 190 (1962).
[5] I. B. Ivanov, D. S. Dimitrov, P. Somasundaran, and R. K. Jain, Chem. Eng. Sci. **40**, 137 (1985).
[6] S. Abid and A. K. Chesters, Int. J. Multiphase Flow **20**, 547 (1994).
[7] R. Tsekov and E. Evstatieva, Prog. Colloid Polym. Sci. **126**, 93 (2004).
[8] B. V. Derjaguin, N. V. Churaev, and V. M. Muller, *Surface Forces* (Plenum Press, New York, 1987).
[9] J. N. Israelachvili, *Intermolecular and Surface Forces* (Academic, London, 1992).
[10] S. G. Yantsios and R. H. Davis, J. Colloid Interface Sci. **144**, 412 (1991).
[11] D. Hewitt, D. Fornasiero, J. Ralston, and L. R. Fisher, J. Chem. Soc., Faraday Trans. **89**, 817 (1993).
[12] J. N. Connor and R. G. Horn, Faraday Discuss. **123**, 193 (2003).
[13] J. Slattery, L. M. C. Sagis, and E.-S. Oh, *Interfacial Transport*

Phenomena (Springer, Berlin, 2007).
[14] L. Y. Clasohm, J. N. Connor, O. I. Vinogradova, and R. G. Horn, Langmuir **21**, 8243 (2005).
[15] R. Tsekov and O. I. Vinogradova, Langmuir **21**, 12090 (2005).
[16] A. M. Cazabat, F. Heslot, S. M. Troian, and P. Carles, Nature (London) **346**, 824 (1990).
[17] S. M. Troian, E. Herbolzheimer, and S. A. Safran, Phys. Rev. Lett. **65**, 333 (1990).
[18] A. Staicu and F. Mugele, Phys. Rev. Lett. **97**, 167801 (2006).
[19] S. Herminghaus, R. Seemann, and K. Jacobs, Phys. Rev. Lett. **89**, 056101 (2002).
[20] V. S. Ajaev, R. Tsekov, and O. I. Vinogradova, Phys. Fluids **19**, 061702 (2007).
[21] V. S. Ajaev and G. M. Homsy, Annu. Rev. Fluid Mech. **38**, 277 (2006).
[22] S. L. Anna, N. Bontoux, and H. A. Stone, Appl. Phys. Lett. **82**, 364 (2003).
[23] R. A. Pushkarova and R. G. Horn, Colloids Surf., A **261**, 147 (2005).
[24] V. G. Levich, *Physicochemical Hydrodynamics* (Prentice-Hall, Saddle River, NJ, 1962).
[25] A. Oron, S. H. Davis, and S. G. Bankoff, Rev. Mod. Phys. **69**, 931 (1997).
[26] J. N. Connor and R. G. Horn, Langmuir **17**, 7194 (2001).
[27] A. Sharma, Langmuir **9**, 861 (1993).
[28] A. V. Lyushnin, A. A. Golovin, and L. M. Pismen, Phys. Rev. E **65**, 021602 (2002).
[29] L. W. Schwartz, R. V. Roy, R. R. Eley, and S. Petrash, J. Colloid Interface Sci. **234**, 363 (2001).
[30] V. S. Ajaev and D. A. Willis, Phys. Fluids **15**, 3144 (2003).
[31] E. Klaseboer, J. P. Chevaillier, C. Gourdon, and O. Masbernat, J. Colloid Interface Sci. **229**, 274 (2000).
[32] S. G. Yantsios and R. H. Davis, J. Fluid Mech. **217**, 547 (1990).
[33] P. N. Brown, G. D. Byrne, and A. C. Hindmarsh, SIAM (Soc. Ind. Appl. Math.) J. Sci. Stat. Comput. **10**, 1038 (1989).
[34] C. Y. Lin and J. C. Slattery, AIChE J. **28**, 147 (1982).
[35] R. Tsekov, P. Letocart, E. Evstatieva, and H. J. Schulze, Langmuir **18**, 5799 (2002).
[36] R. Manica, J. N. Connor, L. Y. Clasohm, S. L. Carnie, R. G. Horn, and D. Y. C. Chan, Langmuir **24**, 1381 (2008).
[37] J. Xu, J. Xia, and Z. Lin, Angew. Chem., Int. Ed. **46**, 1860 (2007).
[38] L. Zhang, S. Maheshwari, H. C. Chang, and Y. Zhu, Langmuir **24**, 3911 (2008).